Sharing Control Strategies for a Hybrid 48V/375V/400Vac AC/DC Microgrid

Carlos Gómez-Aleixandre, Ángel Navarro-Rodríguez, Geber Villa, Cristian Blanco and Pablo García
Dept. of Electrical, Electronics, Systems & Computers Engineering
University of Oviedo, LEMUR Group
Gijón, 33204, Spain
Email: gomeztcarlos@uniovi.es, navarroangel@uniovi.es, villageber@uniovi.es,
blancocristian@uniovi.es, garciafpablo@uniovi.es

***Abstract*—This paper studies the sharing control scheme for a Hybrid 48V/375V/400Vac AC/DC Microgrid, considering reliability as one of the key factors. For that purpose, different possible paths for energy flow provide redundancy to the grid. However, this redundancy leads to the need of enhanced coordinated control systems that can enable these alternative paths for the energy flow. In this paper, both the dc and ac grids are controlled by a P/V droop strategy. At the ac grid, this assumes a main resistive component in the distribution line impedance. The droop control voltage error in steady state is compensated by a novel and simple secondary control approach. The proposed control strategy is based on the calculation of the optimum power flow in each operating point and the real-time modification of the droop characteristics of the converters involved in the power flow calculation. The proposed control is also capable of eliminating the induced voltage drop when using virtual impedance and incorporating any power sharing criteria for the converters contributing to the power production.**

I. Introduction

The future electricity grid is gradually moving in the direction of dc distribution, due the envisaged lower distribution losses (compared with ac distribution) and the more efficient integration of renewables and distributed resources [1]–[3]. The evolution in power electronics and control technologies has enabled the development of dc Low-Voltage (LV) microgrids, which eases the integration of Energy Storage Systems (ESS). Although the pathway from traditional ac distribution systems to these new topologies integrating is not clear, it is reasonable to think that the new grids should take advantage of the already existing ac infrastructure, leading to the creation of hybrid ac/dc microgrids [1]. This hybrid approach should use Power Electronic Converters (PEC) in order to provide redundancy of power flows, thus increasing the grid resiliency [4].

This paper shows a proposal of a hybrid ac/dc microgrid that can be built up over the existence ac infrastructure by adding the corresponding dc energy paths. The coordinated control of all the involved interlinking (ac/dc and dc/dc) converters is also provided, considering a P/V droop control for the primary control and a novel approach for the secondary control.

Secondary control typically relies on integrators or PI regulators to eliminate the voltage deviation, both in ac [5] and dc [6]. This requires periodic calculations for the integrator to operate, gradually reducing the error every cycle. The proposed secondary control is able to eliminate the voltage deviation due to droop controllers based on a single calculation of the optimum power flow, shifting the droop characteristic of each converter according to voltage and power obtained from the power flow, in which any criteria for the power sharing can be used. This proposed solution, requiring only one calculation for optimizing the operating point, has lower communication requirements and robustness against communication delays or loss of transmitted data.

This secondary control also provides the capability of compensating the voltage drop of virtual impedance techniques at the steady-state, [7]–[11]. As stated in [7] the virtual impedance can be used for many different purposes like active stabilization and disturbance rejection or, in the case of droop controllers, for making the line impedance more resistive/inductive, depending on the type of droop used.

However, this virtual impedance causes a voltage drop, that makes the effective total voltage drop greater, since the real output voltage of the converter is lower than the reference one (assuming that the converter is producing power). Some solutions can be found in the literature, like the use of a high-pass filter in the virtual impedance [8] to eliminate the effect of the virtual impedance in steady-state. However, this solution is only valid when the use of the virtual impedance is needed because of its transient effect (like the active stabilization aforementioned). When the steady-state effects of the virtual impedance are also needed, this solution is not valid. It is shown in the paper, how the designed secondary control can take into account this virtual impedance and eliminate the effect of its voltage droop. This is done by adding extra nodes to the optimum power flow calculation and selecting the physical connection of the converter, after the virtual impedance, to be the node having 1 p.u. voltage.

This paper is organized as follows. In Section II, the proposed hybrid microgrid topology and the power converters topologies are described. In Section III, the control strategy

The present work has been partially supported by the predoctoral grants program FPU for the formation in university teaching of Spain MECD under the grant IDs FPU16/05313 and FPU16/06829. This work also was supported in part by the European Union's H2020 Research and Innovation programme under Grant Agreement No 864459 (UE-19-TALENT-864459).

is explained, with a special focus in the proposed secondary control. Section IV shows the simulation results and Section V presents the conclusions.

II. Proposed Microgrid Topology

The hybrid ac/dc network architecture [12] proposed in this paper is shown in Fig. 1 with the topologies of the converters in the shadowed blocks. The ac feeders and the dc lines (both ± 375 and 48 Vdc) are modeled as purely resistive lines, assuming a maximum voltage drop of 5 % at the end of the line for the rated power.

The use of P/V droop control in the ac part of the microgrid is due to the fact that the grid impedance in LV networks is mainly resistive [13]. Being the lines purely resistive, if reactive power loads and references were set to 0, the ac part of the microgrid could be studied as if it was dc. Being the q-axis component of the voltages equal to 0 in steady-state, the d-axis component is equivalent to a dc voltage for the calculations.

For this reason, the analysis done in the paper starts with the dc case, since it is also a simplified study of the ac part. From dc solution, some modifications are done in order to include reactive power and possible non purely resistive impedances in the calculations for the ac complete solution.

As explained in Section I, virtual impedance can be used for different purposes, introducing an induced voltage drop. In this paper, virtual impedance is used for the converters in the ac feeders and is taken into account too for compensating its voltage drop.

III. Coordinated control

As explained in the previous sections, the coordinate control of the power converters is done with a P/V droop control, both for the ac feeders and the 48 Vdc network.

This droop control acts as a primary control, making possible that all the converters which can deliver power, either coming from the connection to the main ac grid or from ESS, contribute to the power sharing.

The power sharing at the primary control level is achieved without requiring communication among the power converters. However, communication among them is used for upper level control, namely secondary and tertiary control for enhanced power sharing. This is later discussed in the paper.

A. ± 375 Vdc grid control

In the ± 375 Vdc grid, the SST provides connection to the mains supply and to the central ESS. In the present paper, this is simplified as a dc/dc converter connected to a dc voltage source since the focus is in the hybrid microgrid. This dc/dc converter controls the voltage different between the positive and the negative bus (750 Vdc) as shown in Fig. 2.

Header PEC (HPEC), connected to node 1, is in charge of the dc bus balancing [14], due to its neutral point clamped topology, assuring that the voltage in both buses is 375 Vdc (one positive and one negative with respect to the neutral).

These two buses are distributed so that loads can be directly connected to these dc buses. They can be connected to either bus, so loads can be strongly unbalanced. Apart from that, Ring#1 PEC is connected to $+375$ Vdc bus and Ring#2 PEC is connected to -375 Vdc bus.

These two buses are distributed, so that loads can be directly connected to them. Due to the different loads at each of the buses (Ring#1 PEC at the $+375$ Vdc and Ring#2 PEC to the -375 Vdc bus respectively), they could become strongly unbalanced thus making much needed the balancing control implemented at the HPEC.

B. 48 Vdc network control

In Fig. 3 the control diagram for the 48 Vdc grid is shown. The control system is separated into two main blocks; 1) the internal converter control and 2) the central control. The internal control implements the voltage control using a quadratic approximation [15] and relies on a cascaded-architecture with an internal current controller. The references for the voltage control are given by a P/V droop. Connected to the internal control, the central controller provides the power references to the different converters based on the secondary control, whose effect is to shift the droop curve.

The droop coefficient for each converter is calculated according to its power rating, corresponding the rated power to a voltage deviation of 10 %. The droop characteristic equation is shown in (1), where k_p is the droop coefficient; P, the measured power output; P_0, the offset power (the one that would correspond to voltage V_0, equal to rated voltage for this paper); V_n and P_n, the rated voltage and power; and V, the output of the droop control.

$$V = k_p(P_0 - P) + V_0 \rightarrow k_p = 0.1 \cdot \frac{V_n}{P_n} \tag{1}$$

C. 400 Vac feeder control

The general control scheme for the converters in the ac feeder is shown in Fig. 4, which is completely equivalent to the 48 Vdc network case except from the decomposition in the synchronous dq reference frame. Details about cross-coupling and feedforward terms shown in [15] are omitted due to space constraints. The reference for the d axis voltage control is given by a P/V droop. The central controller plays the same role as in the case of the 48 Vdc network. In here, also the q-axis voltage reference is provided to the different converters.

D. Secondary control

For the secondary control, a new strategy has been used. The idea consists on changing the P/V droop characteristics of each converter, by modifying offset power P_0 in (1), so that they match the desired solution. For this paper, the chosen solution is to have a power sharing among the droop controlled converters proportional to each converter power rating and a voltage of 1 p.u. at a given specific node. In general, the output of the main converter of the corresponding grid is used as the 1 p.u. reference.

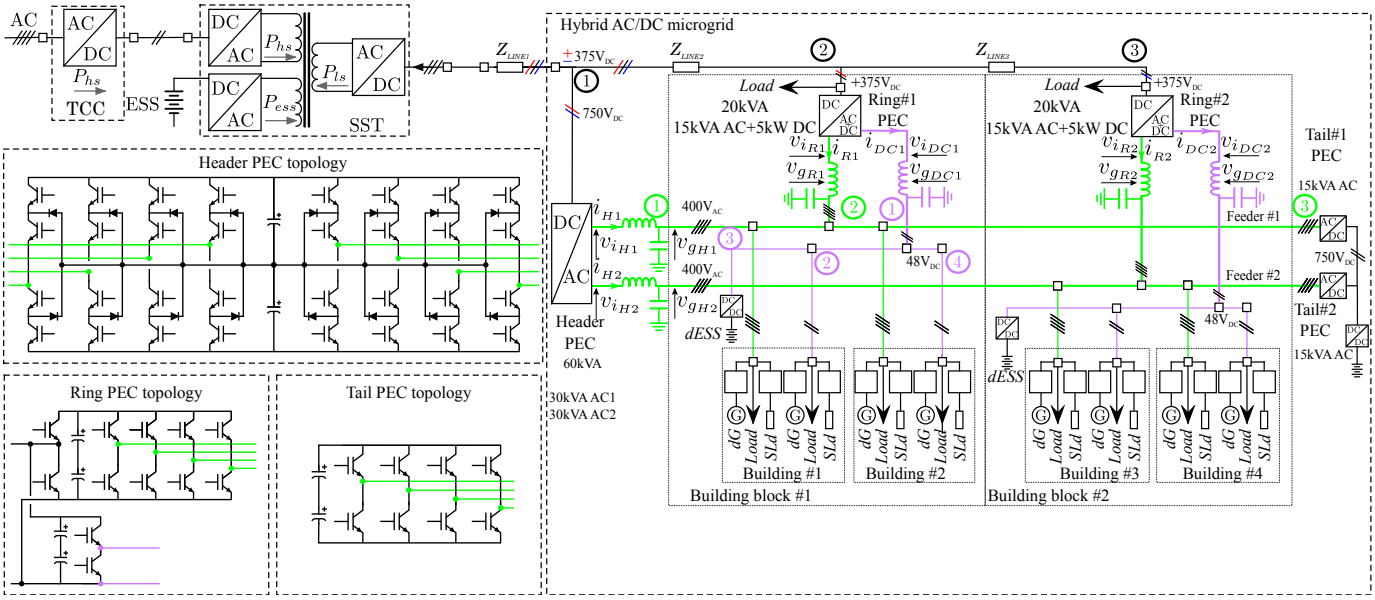

Fig. 1. Proposed system level grid infrastructure [12].

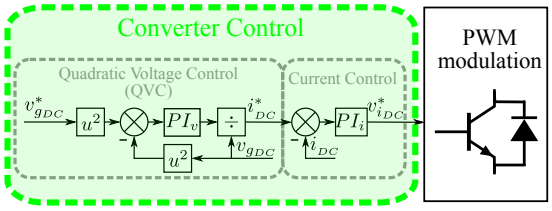

Fig. 2. Control diagram for dc/dc converter used as a simplification for the SST connection to the mains supply and to the central ESS.

This secondary control is applied to the 400 ac feeder and the 48 Vdc network. Considering the proposed grid topology in each case, the loads at each node and the reference output power of each converter, the power flow can be calculated, resulting in the voltage profile at each node considering one of the nodes is set to 1 p.u. For these calculations, only droop-controlled converters participating in the power sharing are taken into account as controllable converters, the remaining are seen as bidirectional loads.

The reference power output of each converter can be selected with different criteria. For the calculations presented hereafter, the sharing among the converters is proportional to the power rating of each converter. If any other criteria is used, this method could easily accommodate to it without further implications.

In this case, as shown in Fig. 1 both studied cases, the ac feeder or the 48 Vdc network, are radial networks, without rings inside. This eases the calculation of the power flow. Different grid topologies, including mesh and ring networks could also be considered, thus increasing the computational burden for the power flow calculations [16].

Calculations required for dc and ac case are very similar, but dc case is presented before, since it is simpler and more straightforward because it does not include reactive power and decomposition of voltage in dq-axis. After presenting both cases, the possibility of including virtual impedance is presented too.

1) Secondary control in dc: Knowing the reference power and the voltage at each converter, obtained from the power flow, P_0 can be calculated so that the droop characteristic, whose equation is shown in (1), meets the requirements. The method is explained using as example a completely linear network, as shown in Fig. 5. The variables shown there have the same names used in the method equations later explained.

In Fig. 6, the flowchart for the method is shown. Step 1 is for initialization, starting assuming no losses. Step 2 to 6 perform an iteration of the power flow. After step 6, a stop criterion is checked for deciding whether to stop or to continue with the next iteration. The stop criterion can be a limit for the difference between the power losses used for the power flow calculation and the ones calculated in step 6, a maximum number of iterations or a mix of both. Step 7 calculates the offset power for each converter, P_{0PECi}, so that the droop curve of each converter matches the solution from the power flow, as shown in Fig. 7. This offset power is sent back to the converter control to modify their droop (see Fig. 3).

2) Secondary control in ac: The implementation of the secondary control in ac is really similar to the dc case but power (S, in this case), voltage, impedance (Z) and currents should all be complex, except for S_{nPECj} which is the nominal power of each converter.

Fig. 8 show the corresponding calculations for ac. The only significant difference is in the last step. Since the droop is applied to P and V_d (real part of S and V complex vectors), the equation for calculating the active power offset only change is to use real part of V. V_q (imaginary part of V for each node) is an output and is sent to the converters as a reference.

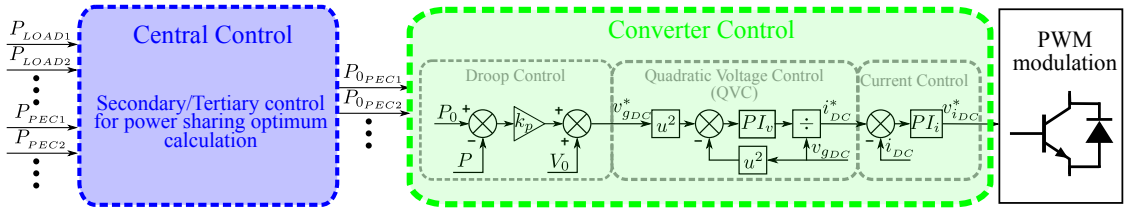

Fig. 3. General control diagram for converters in the 48 Vdc network. P_{LOADi} is the aggregate load connected to node i, P_{PECi} is the measured power output of the converter and $P_{0_{PECi}}$ is the power offset for the converter connected to node i.

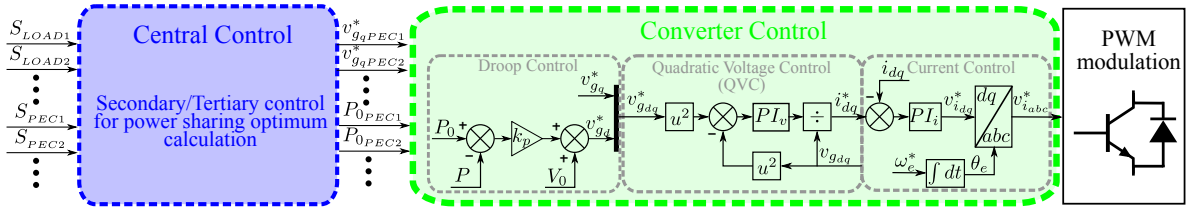

Fig. 4. General control diagram for converters in the ac feeder. S_{LOADi} is the aggregate load connected to node i, S_{PECi} is the measured power output of the converter and $P_{0_{PECi}}$ is the active power offset for the converter connected to node i. Both S_{LOADi} and S_{PECi} mean P and Q are required (being $S = P + jQ$).

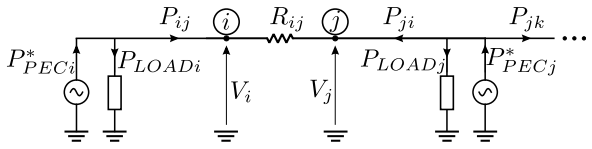

Fig. 5. Power flow diagram. P_{ij} is the power flow from node i to j, P_{ji} from j to i and P_{jk} from j to k. P^*_{PECi}: reference power for converter at node i, P_{LOADi}: total connected load in that node and V_i: voltage in that node.

Apart from the differences due to the use of complex variables in ac, the voltage drop for the dc case is calculated as $2RI = 2R\dfrac{P}{V}$ meanwhile in ac it is $ZI = Z\dfrac{\overline{S}}{\sqrt{3}\cdot\overline{V}}$, because the ac network is three-phase.

3) Secondary control including virtual impedance: As explained in Section II, the aim of the secondary control when virtual impedance is considered is the compensation of the induced voltage drop. Compensating its voltage drop is straightforward with the proposed secondary control, adding extra nodes to the power flow calculations in Fig. 8.

In the example shown in Fig. 8, voltage in physical node 1, V_1, is selected to be 1 p.u., obtaining this voltage at the physical connection of the PEC to that node. A virtual node is added before the virtual impedance voltage drop. This can be seen in Fig. 9 with an example of a circuit including virtual impedance, $Z_{vir,i}$. The voltage in the node in which each converter is physically connected is V_i and it is the one obtained from the power flow explained before. The voltage before the virtual impedance, $V_{PEC,i}$, can be obtained from V_i, adding the voltage drop in the virtual impedance. This calculation is shown in (2).

$$V_{PECi} = V_i + Z_{vir,i}\frac{\overline{S^*_{PECi}}}{\sqrt{3}\cdot\overline{V_i}} \tag{2}$$

The calculated V_{PECi} should be used instead of V_i in last step in Fig. 8. So in Fig. 9, $V_{PEC,i}$, which is a virtual voltage, is the voltage used for the droop calculations but voltage V_i is the one fixed to 1 p.u.

The calculation presented in (2) is done considering a three-phase ac system, but to extend it to dc case is straightforward, by using real (R, P) instead of complex variables (Z, S) and changing the factor of $1/\sqrt{3}$ by factor of 2 for the voltage drop calculation.

IV. Simulation Results

The presented solution has been simulated using Matlab/Simulink. The complete circuit is the one depicted in Fig. 1, with node numbers for each part of the microgrid: green for ac feeder; purple for 48 Vdc network; black for the ±375 Vdc buses.

In the ac feeder, nodes number 1 and 2 have HPEC and the ac output of the Ring PEC (RPEC-AC) with droop control and loads are connected to 2 and 3, where TPEC works in PQ mode.

In the 48 Vdc, the dc output of the RPEC (RPEC-DC) works in droop control, together with a dc/dc converter of 2 kW connected to distributed ESS (dESS-PEC). Loads are connected to nodes 2 and 4.

In the ±375 Vdc grid, HPEC, connected to node 1, are in charge of the dc bus balancing [14] and loads are connected to 2 (positive dc bus) and 3 (negative dc bus).

The details of the different converter rated power and output LC filter parameters as well as the control loop bandwidths and gains are shown in Table I, where PI_i and PI_v are the PI regulators for current and voltage and k_p, the droop coefficient, as shown in Fig. 3 and 4.

The simulation results are presented in two different sections. First, a general result, with different step changes in the loads at each subgrid (48 Vdc/375 Vdc/ 400 Vac), is

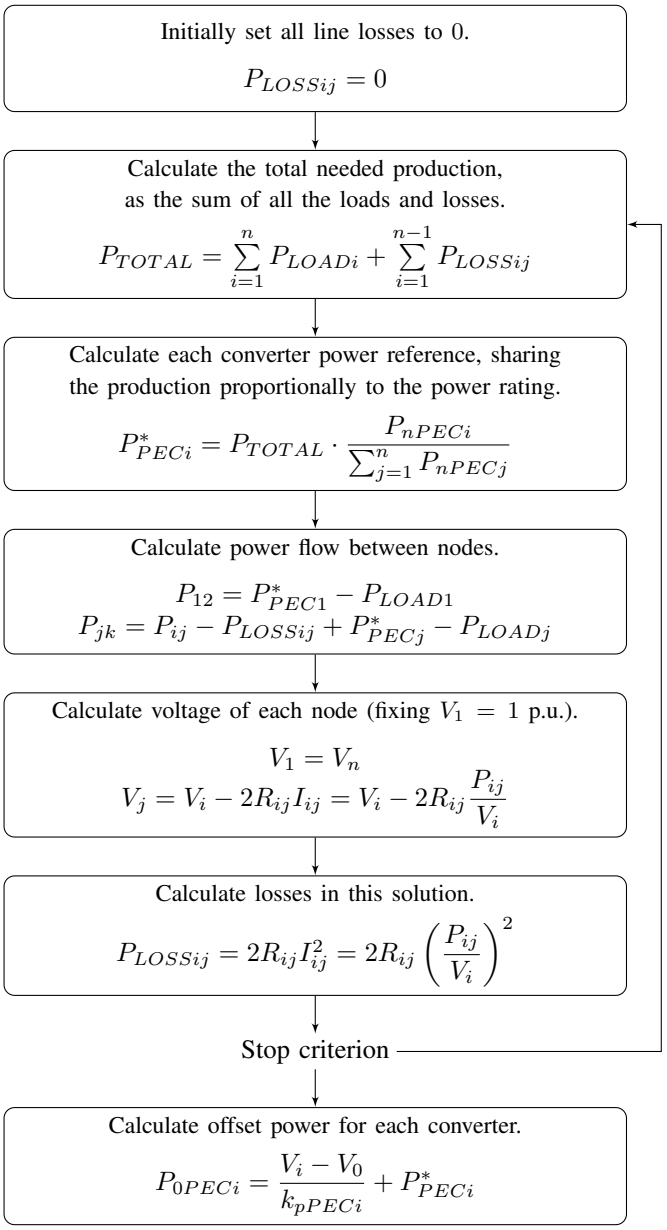

Fig. 6. Flowchart for secondary control in dc. i, j and k denote any three consecutive nodes.

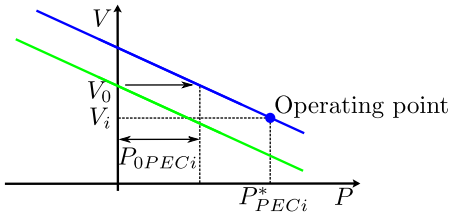

Fig. 7. Droop curve shift for fulfilling power flow solution. Green: base case with $P_{0PECi} = 0$ and blue: final solution.

presented. In this point, the general operation of the grid is shown, together with the activation of the secondary control. Following, a continuation of the simulation for the general

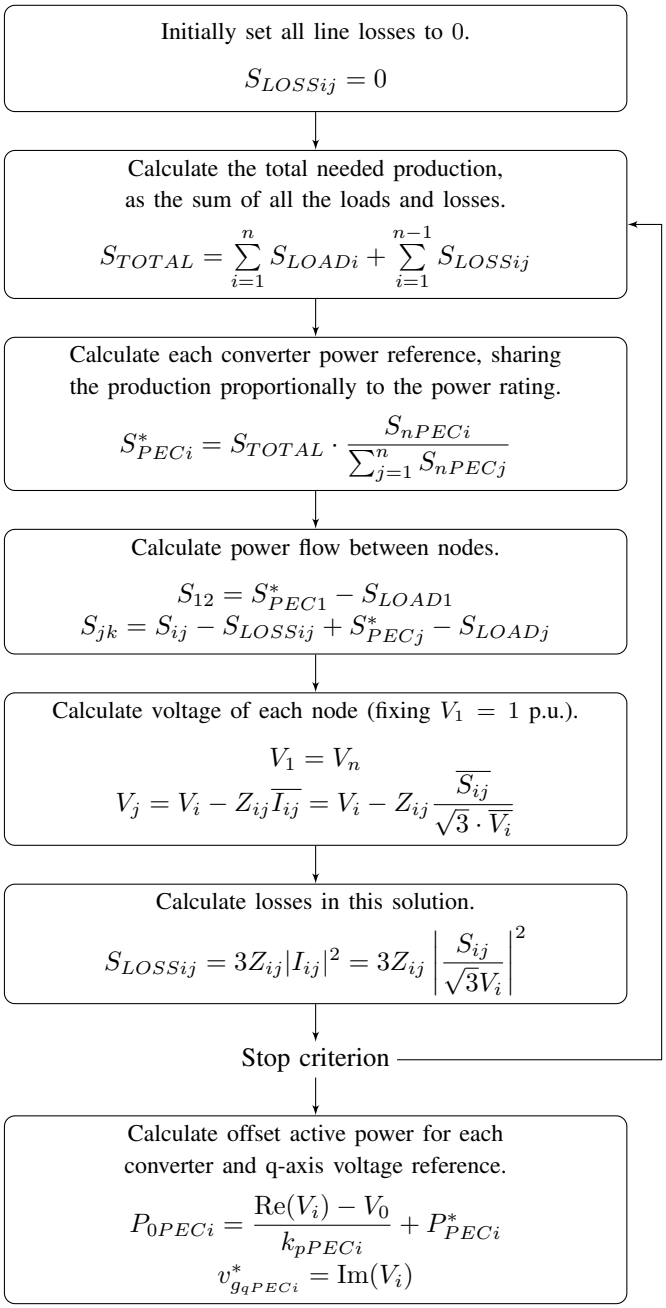

Fig. 8. Flowchart for secondary control in dc. i, j and k denote any three consecutive nodes. For obtaining a more compact expression, active and reactive power equations are presented in its complex form, so they are joint into one equation with $S = P + iQ$, using also $Z = R + iX$. $\overline{x}$, $\mathrm{Re}(x)$ and $\mathrm{Im}(x)$ are the conjugate, real part and imaginary part of a complex vector.

operation of the grid is shown, focusing more in the operation of the secondary control. Different changes are introduced to this secondary control, so that the flexibility of the method is proved.

A. General simulation result

The results for the ±375 Vdc buses are shown in Fig 10. The balancing method from [14] is able to maintain the balance of the dc buses even when having very different demands.

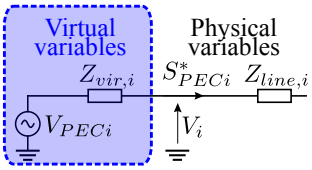

Fig. 9. Example of circuit including virtual impedance. V_i is the voltage at the physical connection of the corresponding PEC and $Z_{line,i}$, the coupling impedance. $Z_{vir,i}$ is the virtual impedance of the PEC and $V_{PEC,i}$, the (virtual) voltage before the voltage drop in the virtual impedance.

TABLE I
CONVERTER PARAMETERS.

Converter	HPEC	RPEC-AC	RPEC-DC	dESS-PEC
S_n / P_n	30 kVA	15 kVA	5 kW	2 kW
L_{filter} (mH)	1.68	3.37	1.47	3.67
R_{filter} (mΩ)	35.3	70.5	30.7	76.8
C_{filter} (mF)	0.5	0.1	5	5
C_{bus} (mF)	5	5	5	5
PI_i: P Gain	5.29	10.58	4.61	11.52
PI_i: I Gain	20.94	20.94	20.94	20.94
PI_i: BW (Hz)	500	500	500	500
PI_v: P Gain	0.111	0.022	1.111	1.111
PI_v: I Gain	222.14	222.14	222.14	222.14
PI_v: BW (Hz)	50	50	50	50
k_p (p.u.)	0.1	0.1	0.1	0.1

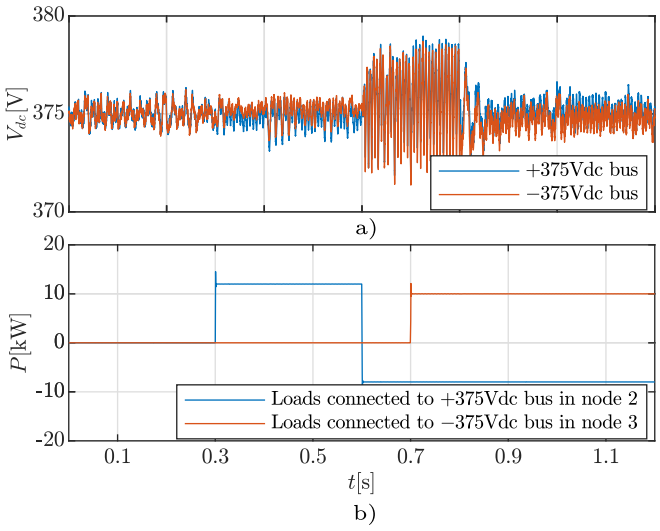

Fig. 10. ±375 Vdc buses simulation result. a) voltage for positive and negative dc buses. b) loads directly connected to both buses.

Fig. 11 and 12 show the results for LV dc network and ac feeder. In both cases, before the vertical line, secondary control is not activated. A sequence of step loads is introduced so that the primary control operation of the system is shown. The vertical line indicates the activation of the secondary control.

LV dc network results are shown in Fig. 11. As expected, the droop control causes a deviation from the nominal voltage. However, when the secondary control is activated, this voltage deviation is eliminated, being the voltage 48.00 V in the end of the simulation, with less than 0.002 % error. This is achieved for node 1, since it was the one selected to have voltage of 1

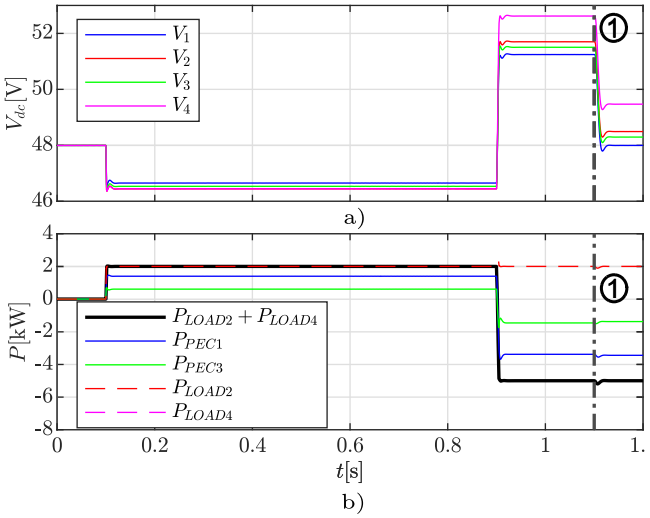

Fig. 11. 48 Vdc grid simulation results. Line 1: activation of secondary control. a) voltage at each node. b) active power production of each converter and active power consumption of each load

p.u. in the power flow solution for this example.

Apart from that, the power sharing between the two converters, gets closer to the theoretical value of 2.5, which is the ratio between both converters rated power. The relationship between power production by converter in node 1 and by converter in node 3 is 2.31 before the secondary control and 2.50 after measured at the end of Fig. 11, with less than 0.04 % error.

The results for the ac feeder are shown in Fig. 12. As commented for the LV dc case, the voltage deviation is eliminated when the secondary control is activated, being 1.00 p.u. at the end of the simulation, with less than 0.06 %. In the ac feeder, the droop-controlled converter uses a virtual impedance approach. As it can be seen, the effect of its voltage drop is also compensated. This is clearly visible since the voltage shown in the figures are measured at the physical converter nodes.

For the power sharing, both active and reactive power have a ratio between both converters of 2, corresponding to the ratio between their rated power. The relationship between active and reactive power production of the converters before the secondary control is activated is 1.28 and 0.86 respectively. After activating the secondary control, it becomes 1.98 for active power (less than 0.95 % error) and 2.03 for reactive power (less than 1.6 % error).

It is worth to remark here that for the reactive power no droop is being used, so the sharing without secondary control is not controlled anyway and depends only on grid configuration and load demand and its distribution in the grid. So, meanwhile P/V droop is able to have an approximation for the active power sharing, which is corrected with the secondary control, no droop is used for the reactive power and the power sharing is controlled only by the secondary control.

In the presented case, the secondary control reference calculation is only done once and the references are sent to the converters. This shows the validity of the method

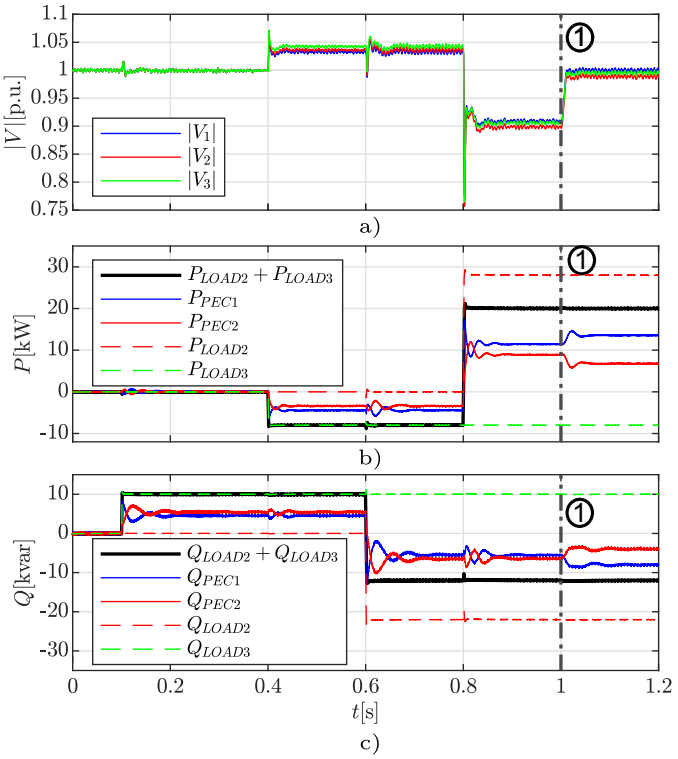

Fig. 12. 400 Vac feeder simulation results. Line 1: activation of secondary control. a) voltage at each node. b) active power production of each converter and active power consumption of each load. c) reactive power production of each converter and active power consumption of each load.

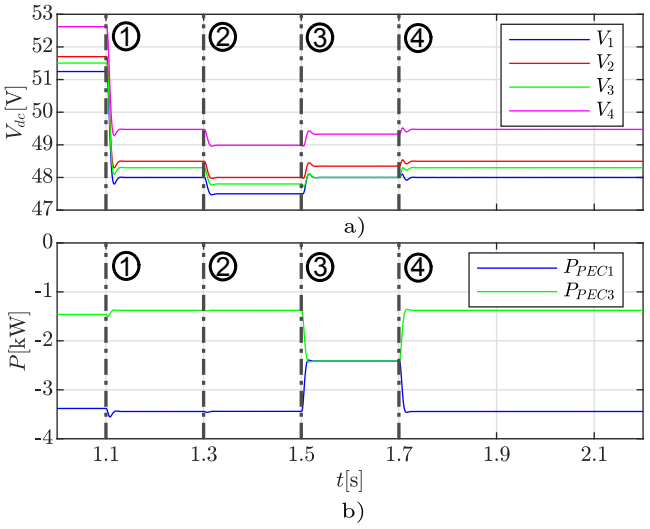

Fig. 13. 48 Vdc grid simulation results for secondary control. Line 1: activation of secondary control. Line 2: change of node whose voltage is set to 48 V, from node 1 to 2 (the change is undone in the line 3). Line 3: change in the power sharing by the converters, from a ratio of 2.5 (proportional to each converter power) to 1 (the change is undone in line 4). Line 4: return to initial situation. a) voltage at each node. b) active power output of each converter.

even for low communication speeds and its robustness against communication delays or loss of transmitted data. However, this is only an example for showing its operation. In a real operation, for taking advantage of the proposed secondary control, the reference calculation and update should be done every time a change in the operating point of the network is detected. Considering low communication speeds, even if significant changes happen between two consecutive checks, the primary control is able to control the operation until the solution is optimized again.

B. Secondary control

For proving the flexibility of the secondary control, an extension of the simulations shown before is presented. Fig. 13 is a continuation of Fig. 11 and Fig. 14 is a continuation of Fig. 12. Power demanded by the loads is not shown, but it remains unchanged from the situation presented in Fig. 11 and 12 when the secondary control is activated.

In both cases, first vertical line indicates the activation of secondary control, that was already shown in the previous figures. The next vertical lines indicate changes in the application of the secondary control, like changes in the node whose voltage is chosen to be 1 p.u. or in the power sharing between the converters. Secondary control reference calculation and transmission is only performed at the time instant represented by a vertical line.

In Fig. 13, starting from the original situation when the secondary control becomes active, a first change is introduced, setting node 2 to have 1 p.u. (48 V) and returning to control voltage in node 1 in the next reference calculation. The second change consists on changing the power sharing among the converters, from a ratio of 2.5, proportional to each converter rated power, to 1, returning to 2.5 in the next reference calculation, thus returning to the initial situation.

It is important to remark here that, when both converters share the power equally, converter in node 3 is working above its rated power. This operating condition is allowed in the simulation for illustrative purposes. With the flexibility shown by the method, it is possible to add more conditions for the power sharing, like these limits for rated power or any other criteria, like ESS State of Charge (SoC).

In Fig. 14, a similar sequence of changes if performed. Starting from the original situation when the secondary control becomes active, a first change is introduced, setting node 3 to have 1 p.u. and returning to control voltage in node 1 in the next reference calculation. For visualizing properly this changes, the original voltage signals are filtered (10 Hz second order filter).

The second change consists on changing the power sharing among the converters, from a ratio of 2, proportional to each converter rated power, to 1, both for active and reactive power. In the next reference calculation, the original power sharing is reestablished for active power and for the last reference calculation it is reestablished for reactive power, returning to the original situation. This shows the flexibility of the method also for having different criteria for both active and reactive power. For example, STATCOM or PEC whose active power is

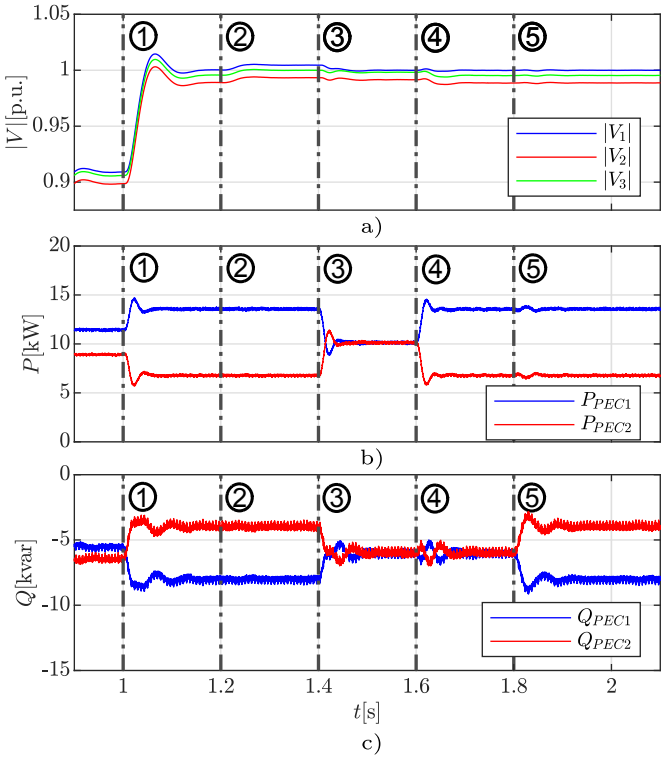

Fig. 14. 400 Vac feeder simulation results for secondary control. Line 1: activation of secondary control. Line 2: change of node whose voltage is set to 1 p.u., from node 1 to 3 (the change is undone in line 3). Line 3: change in the power sharing by the converters, from a ratio of 2 (proportional to each converter power) to 1, both for active and reactive power. Line 4: return to the original power sharing only for the active power. Line 5: return to initial situation. a) voltage at each node. b) active power output of each converter. c) reactive power output of each converter.

fixed for the load they have to feed but whose reactive power can be controlled independently, can participate in the reactive power sharing.

V. Conclusions

This paper has shown a preliminary approach for the sharing control scheme in a novel hybrid ac/dc microgrid. The proposed method enables the different converters to contribute to the power sharing by a droop control implementation. The proposed secondary control eliminates the voltage deviation due to the droop characteristic. It also eliminates the voltage droop caused by the virtual impedance.

Besides that, the secondary control applied in ac allows the reactive power sharing among the converters with no specific droop control. This also eases the integration of converters which are seen as active power loads, but whose reactive power can be controlled to contribute to the sharing, as it can be the case of a converter feeding a load or a STATCOM.

This secondary control is also flexible, because it is easy to introduce any criteria for the power flow solution, like any method for deciding the power sharing among the converters (minimize losses, saturation of converters for its rated power,...) or the possibility of easily changing the node whose voltage is fixed to 1 p.u.

The flexibility of the proposed secondary control allows to introduce new criteria for the power flow solution, like alternative power sharing methods (loss minimization, power limit saturation,...) or the possibility of easily exchange the node with voltage fixed to 1 p.u.

This flexibility eases the integration of additional power sharing mechanism that considers ESS SoC, or the integration of the proposed control system with the tertiary control level.

References

[1] P. Wang, L. Goel, X. Liu, and F. H. Choo, "Harmonizing AC and DC: A Hybrid AC/DC Future Grid Solution," *IEEE Power and Energy Magazine*, vol. 11, no. 3, pp. 76–83, May 2013.

[2] P. Fairley, "DC Versus AC: The Second War of Currents Has Already Begun [In My View]," *IEEE Power and Energy Magazine*, vol. 10, no. 6, pp. 104–103, Nov 2012.

[3] A. Bindra, "Projecting the Evolution of Power Electronics: Highlights from FEPPCON VIII," *IEEE Power Electronics Magazine*, vol. 3, no. 1, pp. 32–44, March 2016.

[4] C. Marnay, H. Aki, K. Hirose, A. Kwasinski, S. Ogura, and T. Shinji, "Japan's Pivot to Resilience: How Two Microgrids Fared After the 2011 Earthquake," *IEEE Power and Energy Magazine*, vol. 13, no. 3, pp. 44–57, May 2015.

[5] J. W. Simpson-Porco, Q. Shafiee, F. Dörfler, J. C. Vasquez, J. M. Guerrero, and F. Bullo, "Secondary Frequency and Voltage Control of Islanded Microgrids via Distributed Averaging," *IEEE Transactions on Industrial Electronics*, vol. 62, no. 11, pp. 7025–7038, 2015.

[6] P. Wang, X. Lu, X. Yang, W. Wang, and D. Xu, "An Improved Distributed Secondary Control Method for DC Microgrids With Enhanced Dynamic Current Sharing Performance," *IEEE Transactions on Power Electronics*, vol. 31, no. 9, pp. 6658–6673, 2016.

[7] X. Wang, Y. W. Li, F. Blaabjerg, and P. C. Loh, "Virtual-Impedance-Based Control for Voltage-Source and Current-Source Converters," *IEEE Transactions on Power Electronics*, vol. 30, no. 12, pp. 7019–7037, 2015.

[8] Z. Liu, S. Ouyang, and W. Bao, "An improved droop control based on complex virtual impedance in medium voltage micro-grid," in *2013 IEEE PES Asia-Pacific Power and Energy Engineering Conference (APPEEC)*, 2013, pp. 1–6.

[9] A. Micallef, M. Apap, C. Spiteri-Staines, and J. M. Guerrero, "Performance comparison for virtual impedance techniques used in droop controlled islanded microgrids," in *2016 International Symposium on Power Electronics, Electrical Drives, Automation and Motion (SPEEDAM)*, June 2016, pp. 695–700.

[10] A. D. Paquette and D. M. Divan, "Virtual Impedance Current Limiting for Inverters in Microgrids With Synchronous Generators," *IEEE Transactions on Industry Applications*, vol. 51, no. 2, pp. 1630–1638, 2015.

[11] J. He and Y. W. Li, "Analysis, Design, and Implementation of Virtual Impedance for Power Electronics Interfaced Distributed Generation," *IEEE Transactions on Industry Applications*, vol. 47, no. 6, pp. 2525–2538, 2011.

[12] C. Gómez-Aleixandre, P. García, A. Navarro-Rodríguez, and G. Villa, "Design and Control of a Hybrid 48V/375V/400Vac AC/DC Microgrid," in *IECON 2019 - 45th Annual Conference of the IEEE Industrial Electronics Society*, vol. 1, Oct 2019, pp. 3977–3982.

[13] J. Rocabert, A. Luna, F. Blaabjerg, and P. Rodríguez, "Control of Power Converters in AC Microgrids," *IEEE Transactions on Power Electronics*, vol. 27, no. 11, pp. 4734–4749, Nov 2012.

[14] C. Wang, Z. Li, X. Si, and H. Xin, "Control of neutral-point voltage in three-phase four-wire three-level NPC inverter based on the disassembly of zero level," *CPSS Transactions on Power Electronics and Applications*, vol. 3, no. 3, pp. 213–222, Sep. 2018.

[15] A. Navarro-Rodríguez, P. García, R. Georgious, and J. García, "Adaptive Active Power Sharing Techniques for DC and AC Voltage Control in a Hybrid DC/AC Microgrid," *IEEE Transactions on Industry Applications*, vol. 55, no. 2, pp. 1106–1116, March 2019.

[16] R. Chai, B. Zhang, J. Dou, Z. Hao, and T. Zheng, "Unified Power Flow Algorithm Based on the NR Method for Hybrid AC/DC Grids Incorporating VSCs," *IEEE Transactions on Power Systems*, vol. 31, no. 6, pp. 4310–4318, 2016.